

PCCP

Accepted Manuscript



This is an *Accepted Manuscript*, which has been through the Royal Society of Chemistry peer review process and has been accepted for publication.

Accepted Manuscripts are published online shortly after acceptance, before technical editing, formatting and proof reading. Using this free service, authors can make their results available to the community, in citable form, before we publish the edited article. We will replace this *Accepted Manuscript* with the edited and formatted *Advance Article* as soon as it is available.

You can find more information about *Accepted Manuscripts* in the [Information for Authors](#).

Please note that technical editing may introduce minor changes to the text and/or graphics, which may alter content. The journal's standard [Terms & Conditions](#) and the [Ethical guidelines](#) still apply. In no event shall the Royal Society of Chemistry be held responsible for any errors or omissions in this *Accepted Manuscript* or any consequences arising from the use of any information it contains.

Monte Carlo simulations of the static friction between two grafted polymer brushes

Ana C. F. Mendonça ^a, Florent Goujon ^b, Patrice Malfreyt ^{*b} and Dominic J. Tildesley ^a

Received Xth XXXXXXXXXXXX 20XX, Accepted Xth XXXXXXXXXXXX 20XX

First published on the web Xth XXXXXXXXXXXX 200X

DOI: 10.1039/b000000x

A configurational bias Monte Carlo method has been developed to study the static friction between grafted polymers immersed in a good solvent. Simple models using the soft quadratic potential from a dissipative particle dynamics study have been used to model polyelectrolytic brushes at physiological pressures (up to 7.5 MPa). Three models of decreasing rigidity have been used to model the friction between the brushes by calculating the tangential component of the pressure induced by a mismatch in the registry of the two grafting surfaces. The static friction coefficient can be calculated for three model systems and the slip between the layers occurs at a much lower values of shear force for the more flexible polymer layer. A moderate increase in the flexibility of the chains reduces the friction coefficient by a factor of *ca.* 20. Tilting the layer directors of the brushes also increases the static friction between the layer when the top, tilted layer is displaced in the direction away from the tilt. Non-equilibrium dynamics techniques for the same model were performed using dissipative particle dynamics and the limiting extremes of the Stribeck curve corresponding to the the boundary lubrication regime and the hydrodynamic lubrication regime were observed for these flat surfaces. As expected, μ_k is significantly lower than μ_s for the same system. The dynamical friction coefficients in the model are in good agreement with those observed in the experiment and the ratio of μ_k/μ_s of between 0.11 and 0.5 observed in the simulations is in reasonable agreement with the value of 0.5 normally observed for these seen for these systems.

1 Introduction

For a fluid confined between surfaces, the friction coefficient (μ) as a function of the relative sliding velocity (v_x) is shown in the Stribeck curve ¹ of Fig 1.

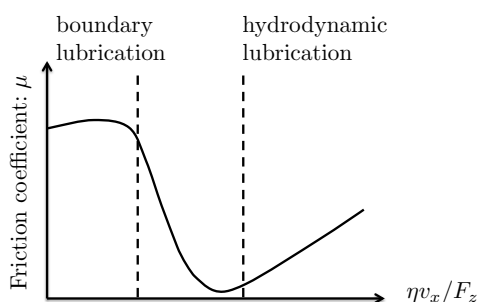


Fig. 1 Representation of the Stribeck curve ², showing the friction coefficient as a function of the sliding velocity v_x .

At high sliding velocity and low normal load, F_z , the system is in the hydrodynamic lubrication regime. For a spherical roller of radius R on a flat surface, the solution of the Navier–Stokes equation ³ shows a linear dependence on v_x .

$$\mu = 2\pi R \frac{v_x \eta}{F_z} \quad (1)$$

where η is the shear viscosity of the entrapped fluid. At lower sliding velocities and higher normal loads, the surfaces are in close contact and the system exhibits boundary layer lubrication (where the limiting value of μ is the static friction coefficient). Between these extremes, there is a mixed or intermediate regime.

At zero sliding velocities, the situation is as shown in Fig 2(a). The layers are aligned along the surface normal and the tangential component of the force is sufficiently small that the polymer layers will distort and may tilt but the surfaces will not move with respect to one another (this is the sticking regime). When the lateral force exceeds a critical value, f_c , the layers slide and the polymers will often tilt in response (this is the sliding regime), see Chapter 9 of Persson ³.

In two recent papers ^{4,5}, we have used the dissipative particle dynamics method (DPD) to calculate the friction coefficient between two flat surfaces coated with polymer and immersed in a solvent. DPD ⁶ is a coarse-grained simulation technique that enables us to use a sufficiently long time-step that

^a EPFL-CECAM, Batochime (BCH), CH-1015, Lausanne, Switzerland

^b Clermont Université, Université Blaise Pascal, Institut de Chimie de Clermont-Ferrand, UMR CNRS 6296, BP 10448, F-63000 Clermont-Ferrand
E-mail: Patrice.Malfreyt@univ-bpclermont.fr

approaches the sliding velocities observed in surface forces experiments on similar systems⁷. In this work, the friction coefficient is calculated at a fixed sliding velocity from the elements of the pressure tensor

$$\mu = -\frac{\langle P_{xz} \rangle}{\langle P_{zz} \rangle} \quad (2)$$

where $\langle P_{xz} \rangle$ is the tangential component and $\langle P_{zz} \rangle$ is the normal component of the pressure. These simulations are in the hydrodynamic lubrication regime over many orders of magnitude of the sliding velocity (see Fig. 2(a) of Goujon *et al.*⁵). The technique models the situation shown in Fig. 2(b) and provides estimates of the kinetic friction coefficient.

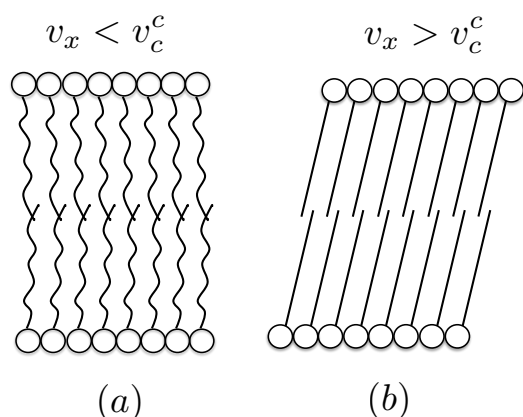


Fig. 2 The change from the regime of (a) static friction to (b) kinematic friction when the lateral force, f_x exceeds some critical force f_x^c

Although, in principal, lowering the shearing velocity in these simulations should allow us to reach the boundary layer regime, in practice as we continue to reduce v_x , the signal for P_{xz} becomes statistically indistinguishable from the noise and we cannot calculate a meaningful value for μ for simulations of 3×10^6 timesteps.

In this paper we propose an alternative simulation approach to measuring μ as $v_x = 0$. We will simulate the static friction coefficient in the situation shown in Fig. 2(a), using a Monte Carlo (MC) approach. We will use an adaptation of the iso-stress, iso-strain simulation MC method developed for studying melting between two solid walls composed of Lennard-Jones atoms^{8,9}. The system consists of two polymer brushes immersed in solvent between two surfaces. The head groups are tethered to a lattice on each surface, the polymer tails are free to move under the intermolecular and intramolecular potentials. The system is prepared by performing MC simulations at constant- μ_{sol}, V, T , where μ_{sol} is the chemical potential of the solvent, followed by constant- P_{zz}, N, T simulations.

This insures both mechanical and chemical equilibrium at a constant load. In the starting configuration, the surface tethering points of the upper and lower polymer layers are in registry with one another. Then, it is possible to perform simulations at constant- P_{xz}, N, T and measure the resulting registry between the two layers. In fact, it turns out to be more efficient to fix the mismatch in the registry of the two surfaces and to measure P_{xz} . These simulations are performed at close contact. There is a thin layer of solvent in the interfacial region between the polymer brushes and additional solvent interspersed within the polymer brush, see Fig 3. The solvent layer is thin enough and sufficiently ordered that it can sustain a shear. As the registry-mismatch is increased by imposing a particular starting configuration, P_{xz} increases, passing through a maximum before the brushes come back into registry. The maximum value of P_{xz} corresponds to the largest value of the lateral pressure that the system could sustain without sliding. The static friction coefficient can be deduced from P_{xz} at this mismatch.

The idea of measuring the degree of registry-mismatch between two lattices to obtain insights on the tribological properties of the materials, has been used in several recent studies¹⁰⁻¹³. The registry index, RI, a parameter that varies between 0 and 1, where 1 corresponds to the worst stacking mode and 0 to the optimal stacking configuration, allows the characterisation of the the sliding-energy landscape and a calculation of the important frictional properties. Using this approach, Hod and coworkers were able to fully reproduce the experimental friction of a graphene nanoflake sliding over a graphite surface¹¹, a Graphene/*h*-BN interface¹³, and also for a non-planar system composed of double walled boron nitride nanotubes¹².

Coarse-grained molecular dynamics (MD) simulations have been used study slip-stick behaviour on surfaces¹⁴⁻¹⁸. Thompson and Robbins¹⁵ studied thin fluid films confined between two solid plates and between crystalline surfaces separated by a molecularly thin layer of linear polymers¹⁷. These simulations are performed on mesoscale models (of a different type than considered in this work) but using sliding velocities that are significantly higher than those that can be attained in the DPD method. In the MC method presented in this work, we are calculating the lateral barrier to movement by measuring the force as a function of layer registry. The dynamical simulations measure the minimum force required to pull the layer over this barrier from a static start until the layers move. So far as we are aware these methods have not been used to reproduce the Stribeck curve.

The problem discussed in this paper is more difficult than those previously tackled by registry-mismatch approaches. The ordering induced by the pinning of the polymers, to fixed positions on the solid surface, does not necessarily transmit structure to the boundary layer because of the orientational and conformational disordering of the polymer chains. To

tackle this problem, we move in stages by defining a simple, rigid DPD model of two rigid polymer layers bound to the surface, comparing the friction with that of the bare surface. We will then relax the rigidity of the polymer by allowing bond-stretching and bond angle deformation introduced using the configurational-bias Monte Carlo method^{19,20}. This will allow us to estimate the effect of conformational flexibility on the friction. We then estimate the static friction coefficient for the different systems, and compare our results with the kinetic friction calculated using the DPD approach of Goujon *et al.*⁵ for the same model, in an attempt to reproduce the Stribeck curve.

2 The potential model

The simulated system consists of two smooth solid surfaces covered with polymer brushes immersed in a good solvent. A DPD model is used in this work, in which the coarse-grained particles are modelled as soft beads. Within a polymer, bonds and angles are modelled using harmonic springs. There are non-bonded interactions between solvent and polymer particles and between the fluid and the wall. Within the same polymer, non-bonded interactions are limited to particles that are separated by more than two bonds.

The total force on a DPD particle i is given by

$$\mathbf{f}_i = \sum_{j \neq i}^N \left[\mathbf{f}_{ij}^C + \mathbf{f}_{ij}^R + \mathbf{f}_{ij}^D \right] \quad (3)$$

which is the sum of the standard, conservative (C), random (R) and dissipative forces (D)⁶. The total conservative force acting between two DPD particles is

$$\begin{aligned} \mathbf{f}_{ij}^C &= a_{ij} \left(1 - \frac{r_{ij}}{r_c} \right) \hat{\mathbf{r}}_{ij} & r_{ij} < r_c \\ &= 0 & r_{ij} \geq r_c \end{aligned} \quad (4)$$

where $r_{ij} = |\mathbf{r}_{ij}|$, $\mathbf{r}_{ij} = \mathbf{r}_i - \mathbf{r}_j$, $\hat{\mathbf{r}}_{ij} = \mathbf{r}_{ij}/|\mathbf{r}_{ij}|$, r_c is the cutoff radius and a_{ij} is the maximum repulsion between particles i and j . The corresponding DPD potential is

$$\begin{aligned} v_{ij}^C(r_{ij}) &= \frac{1}{2} a_{ij} r_c \left(1 - \frac{r_{ij}}{r_c} \right)^2 & r_{ij} < r_c \\ &= 0 & r_{ij} \geq r_c. \end{aligned} \quad (5)$$

In this work, we set $r_c = 1.0$. The wall is modelled as a continuum DPD solid of density ρ_w and the wall-particle force is

$$f_{z,iw} = \pi a_{iw} \rho_w \left(\frac{1}{12} - \frac{z_{iw}^2}{2} + \frac{2z_{iw}^3}{3} - \frac{z_{iw}^4}{5} \right) \hat{\mathbf{z}}_{iw} \quad (6)$$

where $z_{iw} = |z_i - z_w|$ with $z_w = \pm L_z/2$ and a_{iw} is the repulsion parameter between the solvent or polymer particle and a

wall-DPD particle in the continuum solid. The derivation of eqn (6) is given in Appendix A.

The spring force between two connected polymer particles is

$$\mathbf{f}_{ij}^S = -k_s(r_{ij} - r_0) \hat{\mathbf{r}}_{ij} \quad (7)$$

where r_0 is the equilibrium bond-length and k_s is the spring constant.

The angle θ_{ijk} is the internal angle defined between three polymer particles, i , j , and k . The force on particle i from the bond-angle potential,

$$v(\theta_{ijk}) = \frac{1}{2} k_\theta (\theta_{ijk} - \theta_0)^2, \quad (8)$$

is²¹

$$\mathbf{f}_{i,\theta_{ijk}} = \frac{k_\theta (\theta_{ijk} - \theta_0)}{\sin(\theta_{ijk})} \left[\frac{\mathbf{r}_{kj}}{D} - \frac{S \mathbf{r}_{ij}}{D r_{ij}^2} \right] \quad (9)$$

where $S = \mathbf{r}_{ij} \cdot \mathbf{r}_{kj}$, $D = r_{ij} r_{jk}$, k_θ is the angular spring constant, and θ_0 is the equilibrium value of the bond angle.

Throughout this paper the unit of mass, m , the cut-off distance, r_c and the reduced temperature are set to one. The interaction parameter a_{ij} for solvent-solvent is set to 25. For the solvent-polymer interaction, a_{ij} is set to 20; the slightly lower value encourages the brushes to extend in the presence of a good solvent²². a_{ij} for the non-bonded interaction *within* polymers is set to 75; a larger value of a_{ij} helps to maintain the rigidity of the polymer brushes.

In eqn (6), a_{iw} is set to 83.0 and ρ_w is set to 8.0. The spring constant for the polymer bonds, k_s , is set at 200 and the equilibrium distance, r_0 , is set to 0.8. For the bond angles, k_θ is set to 400 and the equilibrium angle, θ_0 , is set to π . A lower value of k_θ was also tested, $k_\theta = 200$, to understand the influence of this parameter on the rigidity of the brushes and consequently on the results.

3 Simulations

The initial simulation box is a rectangular parallelepiped with dimensions $L_x = L_y = 9$ and $L_z = 17.5$. The starting configuration was composed of $N_s = 2600$ solvent particles confined between two walls, each composed of one layer of $N_w = 324$ particles rigidly fixed in the configuration of the (100)-plane of the body-centered cubic (bcc) lattice, with a lattice spacing of 0.5. The walls are parallel to the x and y planes, separated by a distance L_z . We note that these wall particles are used to define the anchoring positions of the polymers but that the only wall potential is that given by eqn (6). Polymer brushes were end-grafted to each of the boundary walls to give a total of $N_p = 162$ polymers, each polymer composed of $N_b = 10$ monomers.

This work aims to mimic the surface force balance (SFB) experiments of Chen *et al.*⁷ of bio-compatible polyzwitterionic brushes of poly[2-(methacryloyloxy) ethyl phosphorylcholine] (pMCP), in aqueous media. The experiments show that these brushes produce extremely low coefficients of friction (in the order of 10^{-3}) at physiological pressures (up to 7.5 MPa), with corresponding applications in biomedical devices and *in-vivo* boundary lubrication. In our model, each polymer particle corresponds to ca. five monomers of MPC. The cut-off radius (r_c) was set 2.2 nm, a value chosen taking into account the approximate length of one monomer of polymer and the fact that each DPD polymer bead was composed of five monomer units. This corresponds to 185 molecules of water coarse-grained in each solvent bead. The polymers are grafted uniformly at the surface at a surface coverage of 0.25. The interchain distance at the grafting point is $\ell = 1.0$, assuring that the ratio between the unperturbed brush height and the interchain distance is close to the one determined in the experiment of Chen *et al.*⁷.

Polymers are constrained to align at a fixed angle to the top and bottom walls. The angle between the anchoring point on the wall and the first polymer bead can be set to a chosen value, with $\theta_0 = \pi$ corresponding to the layer director normal to the surface. Periodic boundary conditions are applied in the x and y directions, with the walls confining the fluid in the z direction. The wall potential is sufficiently repulsive to prevent solvent particles escaping from the pore.

The approach used in this paper to predict the static friction coefficient uses the calculation of a tangential component of the pressure, namely $\langle P_{xz} \rangle$. This component is normally zero in systems at the equilibrium unless there is a sufficiently strong inhomogeneity in a static external field along the x -direction. This approach contrasts with our previous work, where we have attempted to calculate the friction coefficients at very low shearing velocity using a non-equilibrium DPD method. Unfortunately, at very low shear rates (less than 10^{-4}) the mean value of P_{xz} is small compared to the estimated error, even for extremely long simulations runs of the order of 10^6 time steps⁵ and it is impossible to extract the friction coefficient.

It was initially unclear if we would-be able to extract an off-diagonal element of the stress from our MC simulations. A non-zero $\langle P_{xz} \rangle$ depends on a non-zero static external field along x (the direction parallel to the interface). This field depends on the order induced by the grafting of the polymers at the wall and the incommensurability of the two polymer surfaces. In the case of chains, oriented perpendicular to the surface, these two effects create a small x -dependent field across the gap between the brushes. This field can easily be lost if the chains are disordered through their internal flexibility (that is the bond length, bond angle and dihedrals variations). In this case the ordering of the tethering points is not transmitted to

the boundary layer. We have considered the effect of chain disordering by building three models of different rigidity: a model with two completely rigid polymer combs separated by several monolayers of solvent, (the *rigid* model); a model in which the bonds lengths of the polymers are allowed to fluctuate so that average height of the polymer brush can change (the *semi-rigid* model); and a model in which both the bond angles and bond-lengths are allowed to fluctuate (the *fully-flexible* model). Each one of these models was studied in systems where the polymer brushes grow perpendicular to the grafting surfaces, and also in systems where all the polymer brushes are tilted in the x -direction, so that the director of the layer forms an angle of 30° in respect to the walls. A representation of the *fully-flexible* model in both the tilted and the untilted systems can be seen in Fig. 3. The study of the system in which the overall polymer chains are tilted in their equilibrium geometry allows us to explore the effect of increasing the field in the x -direction. A recent study by Laurson *et al.*²³ suggests that in the boundary lubrication regime there is a close relation between friction force and the detailed orientation and structure of the confining surfaces.

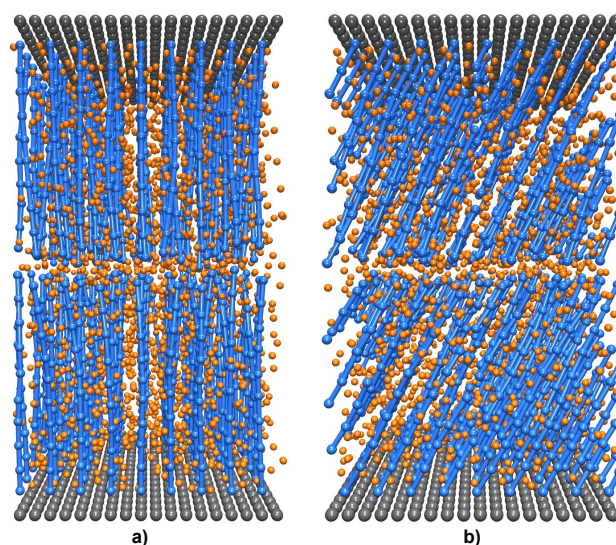


Fig. 3 Snapshot of the *fully-flexible* model in a system where the polymer brushes: a) are perpendicular to the grafting walls and b) are tilted by an angle of 30° in respect to the surfaces. The solid surfaces are represented by a layer of DPD particles separated by L_z , where N_p polymer chains composed of N_b units each are end-grafted. The polymers are immersed in N_s solvent particles.

The initial configuration was generated from the *rigid* model, equilibrated at constant-NVT, for 80000 cycles. The result, was the starting point for the simulations in the *semi-rigid* and *fully-flexible* systems. Each MC cycle consists of one attempted translation of all solvent particles. In the *semi-rigid*

and *fully-flexible* cases, there is an additional attempt to recreate all the adsorbed polymer chains using the configurational bias technique (CBMC). The CBMC was implemented using the method of Smit²⁰. In creating a new polymer chain, each successive particle is added from the previous particle (starting at the anchoring point). For each addition to chain, $k = 30$ trial positions were sampled around the previous particle. The length of the bond in each trial k is chosen by sampling from the distribution $r^2 \exp(-\beta v^s(r_{ij}))$. In the *fully-flexible* brushes system, the polar angle for the new bond with reference to the previous bond is given by calculating the bond angle energy. First we generate a random vector on a unit sphere and determine the angle θ . This vector is accepted with a probability $\exp(-\beta v(\theta_{ijk}))$, and if rejected the procedure is repeated until a value of θ has been accepted. This acceptance-rejection method is shown to give the desired distribution of trial orientations.

Once the probability distribution, ρ_k , for the k trial points is calculated from the interaction of each trial particle with the solvent, the wall and for all the other non-bonded interactions within the polymer, one of the trial states is chosen by sampling from ρ_k . The entire polymer is built in this way. The new polymer configuration is accepted with a probability given by

$$\min\left(1, \frac{W_{\text{new}}}{W_{\text{old}}}\right) \quad (10)$$

where W_{new} is the Rosenbluth weight of the new trial polymer (the product of the weights for each addition along the chain) and W_{old} is the Rosenbluth weight of the old polymer calculated by a deconstruction of the old chain.

Each system was simulated at constant- μ_{sol}, VT , by creating and destroying solvent particles at a fixed $\mu_{\text{sol}} = 11.5$, to produce a density of solvent, $\rho_{\text{sol}} \approx 3$. The details of the grand canonical simulations can be found in Goujon *et al.*^{5, 24}. The constant $\mu(z)$ profile across the box is checked using the Widom test-particle method²⁵.

The simulations were then continued at constant- $NP_{zz}T$, by allowing the box length to fluctuate along the z -axis according to the applied load (P_{zz}) and scaling the positions of all mobile particles in the solvent and in the polymer. Then, NVT simulations were performed to relax the systems at this new volume, and to produce the starting configuration for the subsequent iso-stress (constant- P_{xz}, N, T) simulations. The pressure tensor in the fluid is calculated using the Irving-Kirkwood definition^{26,27}

$$P_{\alpha\beta}(z) = \langle \rho(z) \rangle k_B T + \frac{1}{\mathcal{A}} \left\langle \sum_{i=1}^N \sum_{j>i} \frac{(\mathbf{r}_{ij})_\alpha (\mathbf{f}_{ij})_\beta}{|z_{ij}|} \times \theta\left(\frac{z_i - z}{z_{ij}}\right) \theta\left(\frac{z - z_j}{z_{ij}}\right) \right\rangle \quad (11)$$

where the pressure is calculated in slabs of thickness Δz centred at z and the $i - j$ pair contributes to all slabs between i and j . $\rho(z)$ is the density of the particles along z , $z_{ij} = z_i - z_j$, T is the temperature, $\mathbf{1}$ is the unit tensor, $\mathcal{A} = L_x \times L_y$ and $\theta(z)$ is a unit step function. A fraction $\Delta z/|z_{ij}|$ of $\mathbf{r}_{ij} \cdot \mathbf{f}_{ij}$ is added to all the slabs between particles i and j . Note that the force on i from j includes terms associated with the wall potential, the bond stretching potentials and bond angle potentials within the polymers. In the case of 3-body-forces such as $\mathbf{f}_{i,\theta_{ijk}}$, then the contribution for a given angle θ_{ijk} is $\mathbf{r}_{ij} \cdot \mathbf{f}_{i,\theta_{ijk}} + \mathbf{r}_{kj} \cdot \mathbf{f}_{k,\theta_{ijk}}$ ²⁸.

Several values of the P_{zz} were used with the aim of obtaining approximately one monolayer of solvent between the upper-wall and the lower-wall brushes. Our objective was to understand the dependence of the frictional component of the pressure tensor, P_{xz} , as a function of the applied load. For the *rigid* model, we used $P_{zz} = 25, 27$ and 29 in reduced units. In the case of the *semi-rigid* and *flexible* models, values of $21, 22, 23, 25$ and 27 were employed. Higher values of P_{zz} were needed in the *rigid* polymers system in order to obtain the monolayer, then in the cases of the *semi-rigid* and *fully-flexible* systems.

The normal pressure calculated from eqn (11) is constant across the slab (see Fig. 9) and is equal to the imposed pressure in the constant- $NP_{zz}T$ simulation. In reduced units, pressure is defined as $P^* = Pr_c^3/k_B T$, and therefore for a temperature of 298 K, a reduced pressure of 23 corresponds to 9 MPa, a value close to the mean contact pressures observed experimentally⁷.

In this work a quasi-static approach is used to study friction at zero shear-rate. As the top and bottom walls are displaced, the attached film passes through a succession of equilibrium states^{8,9,29}. The lateral component of the pressure tensor at each equilibrium state, P_{xz} , arises from the relative displacement of the brushes creating a static external force depending on the degree of alignment. This technique allows to study the behaviour of the fluid in the stick regime and to determine the origin and nature of the stick-slip transition. The position of the polymer anchoring points are

$$\begin{aligned} x_i^{[2]} &= x_i^{[1]} + \alpha\ell \\ y_i^{[2]} &= y_i^{[1]} \\ z_i^{[2]} &= z_i^{[1]} + L_z \end{aligned} \quad (12)$$

where ^[1] and ^[2] represent the lower and the upper wall respectively, ℓ is the lattice constant (in this case the same as the inter-chain distance) and $\alpha\ell$ specifies the relative lateral alignment of the wall in x . In the initial simulation ($\alpha = 0.0$) the top and bottom polymers are in registry. Then, α is incremented in small steps of $\Delta\alpha$ (by displacing the upper wall in the x -direction while the lower wall remained fixed), until the walls were completely out of registry at $\alpha = 0.5$. A sketch of the model system can be seen in Fig. 4. An independent MC simulation of 60000 cycles was performed for each value of

α at constant L_z , storing configurations every 10 cycles. Each MC simulation for a given α was initiated from an equilibrated configuration where the walls were completely in registry.

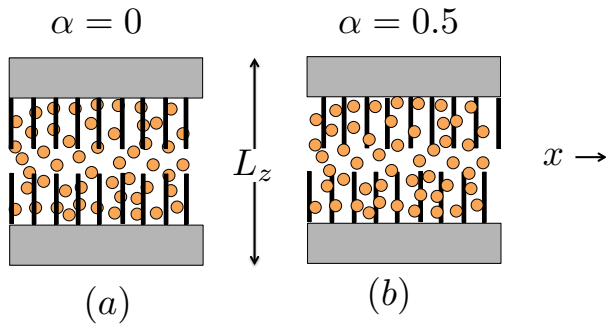


Fig. 4 Sketch of the model system. (a) At $\alpha = 0.0$ the surfaces are in registry and (b) at $\alpha = 0.5$ they are completely out of registry. The solid black lines represent rigid tethered polymers and the solvent particles are shown in orange.

The untilted *flexible* model was also studied by non-equilibrium DPD simulations. The same starting configuration was used in both CBMC and DPD. We also used the same conditions (T , L_z , N_s) and a_{ij} interaction parameters in both methods. In the DPD approach, the \mathbf{f}_{ij}^R and \mathbf{f}_{ij}^D components of the total force \mathbf{f}_i defined in Eq. 3, are given by

$$\mathbf{f}_{ij}^R = \sigma \omega^R(r_{ij}) \theta_{ij} \frac{1}{\sqrt{\delta t}} \hat{\mathbf{r}}_{ij} \quad (13)$$

$$\mathbf{f}_{ij}^D = -\gamma \omega^D(r_{ij}) (\hat{\mathbf{r}}_{ij} \cdot \mathbf{v}_{ij}) \hat{\mathbf{r}}_{ij} \quad (14)$$

where σ and γ are the noise strength and the dissipation strength, respectively. θ_{ij} is a random Gaussian number with zero mean and unit variance, $\mathbf{v}_{ij} = \mathbf{v}_i - \mathbf{v}_j$ is the relative velocity, and δt is the time step. Here, δt was set to 0.01 (equivalent to 1 ps).

The terms $\omega^R(r_{ij})$ and $\omega^D(r_{ij})$ are dimensionless weighting functions. According to Espanol and Warren³⁰, a system will sample the canonical ensemble and obey the dissipation-fluctuation theorem if

$$\gamma = \frac{\sigma^2}{2k_B T} \quad \text{and} \quad \omega^D(r_{ij}) = (\omega^R(r_{ij}))^2 \quad (15)$$

where k_B is the Boltzmann constant and $\omega^D(r_{ij})$ is equal to $(1 - r/r_c)^2$.

The shear rate, $\dot{\gamma}_a$, is applied to the system by moving the top and bottom walls in opposite directions along x . Several simulations were performed at different $\dot{\gamma}_a$ and L_z , more specifically, $\dot{\gamma}_a = 2.5 \times 10^{-4}$, 5.0×10^{-4} , 1.0×10^{-3} for each $P_{zz} = 23, 25$ and 27 . In this study, the shear rates are in the range of $10^{-4} - 10^{-3}$ in reduced units, which correspond to real shear rates of the order of 10^6 s^{-1} , for the time step used in these simulations. We have chosen to use the small as possible values of shear rate, that still allowed accurate estimates of the friction coefficient, to compare with the zero-shear values calculated from the MC method. Additional details of the DPD simulations are given in Goujon *et al.*⁴.

4 Results and discussion

Three model systems of end-grafted polymer chains immersed in a good solvent and confined between two planar walls (Fig. 3) are simulated using the CBMC method. The *fully-flexible* system was also studied by DPD simulations at low shear rates. Our aim is to predict the friction in both the boundary-layer lubrication and the hydrodynamic regimes of the Stribeck curve (Fig. 1)

The rigidity of the polymer brushes and the presence of a monolayer of solvent in the gap between the upper-wall and lower-wall grafted polymer brushes, are two important conditions for the calculation of a non-zero frictional force. Figure 5(a) shows the density profiles of the polymer brushes and the solvent along the z -direction (normal to the interface), for the *fully-flexible* case. A single layer of solvent is present in the region between the brushes, corresponding to the small peak in the middle of the pore. The density profile $\rho(z)$ for the beads of the polymer exhibits ten clear peaks in each layer. The density profile of the last four monomers of each polymer (i.e. those closest to the middle of the box) is shown as a function of x (the direction parallel to the surface) in Fig. 5(b) at $\alpha = 0.5$. Even when the surfaces are completely out of registry, and despite the fluctuations in the the bond lengths and angles, the polymers are sufficiently rigid to create residual ordering of the tails in the $x - y$ plane between the brushes and this gives rise to a non-zero value of P_{xz} . Although these average densities create the picture of a highly ordered interface, a top view of the system at $\alpha = 0.0$ and $\alpha = 0.5$ (Fig. 6(a) and Fig. 6(b), respectively) shows some of the disorder in the fully flexible model. In this instantaneous picture of the system, the dark- brushes are grafted to the upper-wall, the light-blue ones to the lower-wall and the red particles correspond to the anchoring points in the upper wall. The disordering is more pronounced at $\alpha = 0.5$ but clearly present in both cases.

The internal structure of the adsorbed polymer can be gauged from the distribution of bond-lengths and angles. The

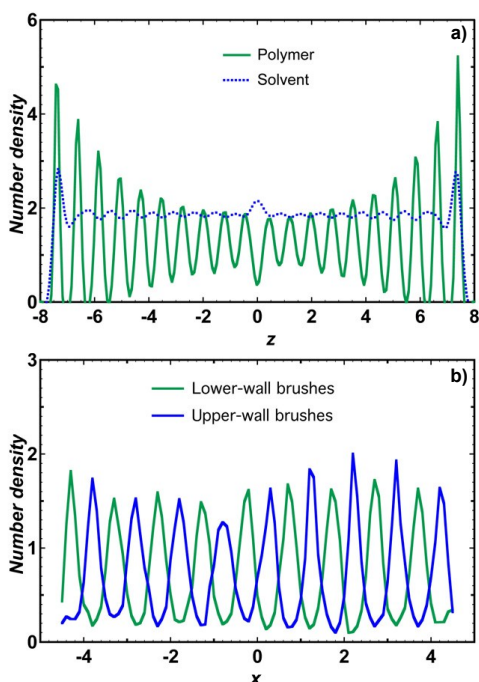


Fig. 5 Number density profiles for: a) polymer brushes and solvent along the surface normal; b) the last four monomers of each polymer brush along the direction parallel to the surface, for a wall registry of $\alpha = 0.5$. For the *Fully-flexible* model at $\langle P_{zz} \rangle = 23$

distribution of bonds for the *fully-flexible* system at three different normal pressures is shown in Fig. 7(a). The average bond-length decreases as P_{zz} increases. This shift in the peak of the distribution with respect to the underlying Gaussian distribution (dashed line) is due to significant repulsion between the brushes on opposite sides of the pore as the imposed pressure increases and the pore-width decreases by 0.3 as P_{zz} changes from 23 to 25.

Fig. 7(b) shows the distribution of the bond-angles, for the *fully-flexible* system using different angular spring constants: $k_{\theta} = 200$ and $k_{\theta} = 400$. The distribution peaks are close to the underlying normal distribution (dashed lines) with $\theta_0 = \pi$. The small variation in θ along the length of the chain creates much of the disorder shown in Fig. 6. We have taken some care to study the ordering in the *fully-flexible* model, it is obvious that the *rigid* and *semi-rigid* models will be more strongly ordered at the interface between the brushes. In considering the static friction, we will start with the rigid model, where we are likely to see the the largest values of $\langle P_{xz}(z) \rangle$ and hence friction and then relax the constraints on the polymers by considering the other two models. Fig. 8(a) shows $\langle P_{xz}(z) \rangle$ as a function of α , for the *rigid* system at $\langle P_{zz}(z) \rangle = 29$ (for simplicity, we take $P_{\alpha\beta} \equiv \langle P_{\alpha\beta} \rangle$ from now on and the ensemble

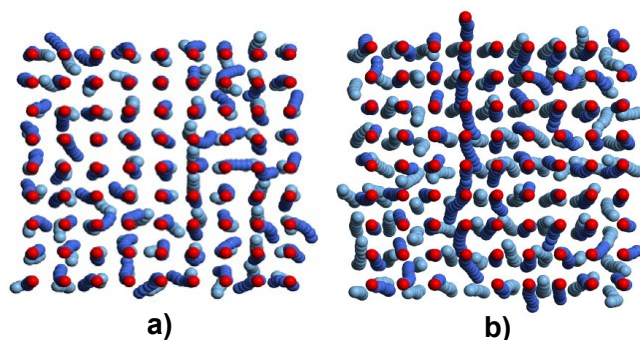


Fig. 6 Top view of the system at: a) $\alpha = 0.0$ and b) $\alpha = 0.5$. Upper-wall polymer brushes are represented in dark blue and lower-wall polymer brushes are in light blue. The red beads correspond to the anchoring point in the upper wall.

averages will be understood). The $P_{xz}(z)$ profiles are presented in Fig. 8(b), for each different α . We note the P_{xz} values are constant and non-zero in the middle of the pore and 0 elsewhere. The values in the middle of the pore that are used to construct the curve in Fig. 8(a). We note that the $P_{xz} = 0$ away from the interface is the result of the symmetry of the rigid polymer system, which means there is no net field in the x -direction away from the region between the brushes. This is not the case for a rigid tilted system of polymers or when there is sufficient disorder associated with the bond-length and bond-angle fluctuations.

As α increases from 0.0 to 0.5, P_{xz} increases from zero to a maximum, also called the static friction point, with coordinates $(\alpha_{\text{yield}}, P_{xz}^{\text{yield}})$. As first suggested by Gee *et al.*³¹, when two surfaces are pushed close together and the space between them is occupied by only few layers of solvent, then sliding cannot be initiated until a critical stress (or yield stress, P_{xz}^{yield}) is exceeded. The walls then slide over one another and eventually come back to the rest point until the critical stress is once again attained, and the walls again slip over one another. This stick-slip cycle suggests that the structure of the system induces the formation of a solid-glassy film when the walls are in registry, and that the film will melt when walls are moved out of registry. Such behaviour has been observed in simulation by Schoen *et al.*⁸ for a simple system composed of two perfectly crystalline walls with a few layers of liquid between them. In this study, we find a similar behaviour in adsorbed polymer systems for each of the three models considered. The *rigid* model corresponds to the structured static surface studied by Schoen *et al.*⁸, whereas the the *fully-flexible* model corresponds to inhomogeneous polymer surfaces confining a monolayer of solvent. After the yield point, P_{xz} decays monotonically to zero at $\alpha = 0.5$. Note that although $\alpha = 0.5$ corresponds to the surface out of registry, because of the symmetry

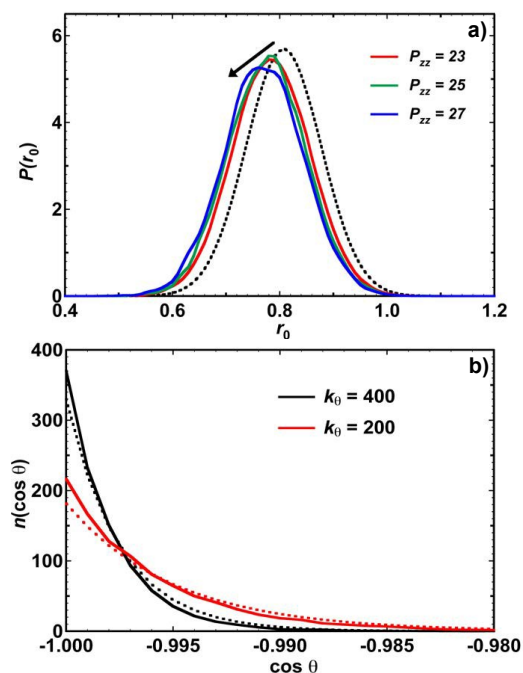


Fig. 7 a) Distribution of bond-lengths sampled from the underlying distribution $r_{ij}^2 \exp(-\beta v^s(r_{ij}))$, for three different values of P_{zz} ; b) distribution of bond angles sampled from $\exp(-\beta v(\theta_{ijk})) \sin(\theta_{ijk})$, for simulations at two different values of k_θ . The underlying distributions are shown as dashed lines.

of the anchoring points the net force on the lower surface from the displaced upper surface is zero. For $0.5 < \alpha < 1$, the system will behave in the same way as for $0.0 < \alpha < 0.5$, but with $P_{xz} < 0$. At $\alpha = 0.5$ the film between the brushes is metastable and a small displacement in either direction will be opposed by a tangential force of the opposite sign. The portion of the curve for $0.5 < \alpha < 1.0$ has the same shape but the opposite sign to the portion for $\alpha = 0.0$ to 0.5 . In contrast, the normal pressure tensor $P_{zz}(z)$ in these systems is constant across the pore, as it must be for mechanical stability.

Turning to the *fully-flexible* model, Fig. 9(a), shows the normal pressure broken down into its various components at an imposed load of $P_{zz} = 23$. The pressure is the sum of the kinetic, conservative, bonds and angles contributions. A strong oscillation is seen in a number of these profiles. However, as expected, the total $P_{zz}(z)$ profile is flat and its average value corresponds to the imposed $P_{zz}(z)$, for all α . Fig. 9(b) shows a typical $P_{xz}(z)$ profile for the fully flexible model, along the z -direction.

The simulation consisted of 50000 MC cycles stored at intervals of 10 steps. The 5000 stored configurations were used to construct 100 block averages which were used to estimate

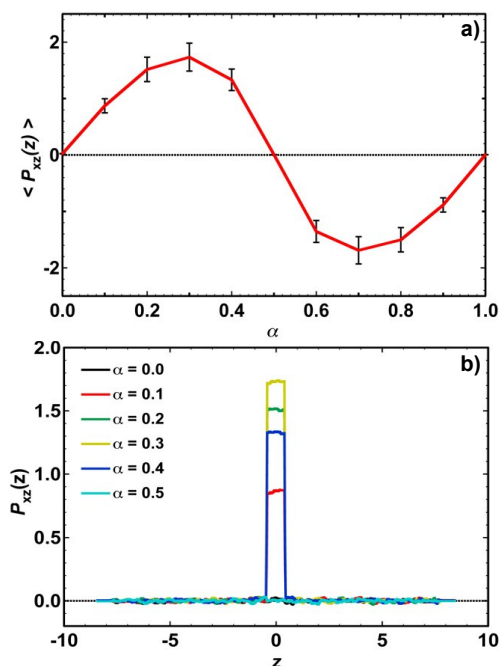


Fig. 8 Frictional pressure profiles: a) $P_{xz}(z)$ as a continuous function of the registry of the rigid walls, α ; b) $P_{xz}(z)$ calculated through the IK definition, for $0.0 < \alpha < 0.5$, for the rigid system.

the standard error in the mean. The maximum in the centre of the box corresponds to the region between the brushes, it is what remains of the flat step Fig. 8(b) for the *rigid* model. The non-zero value of P_{xz} away from the interface is the result of the chain disordering through bond stretching, bond-angle and torsional distortions. A maximum value of P_{xz} corresponding to P_{xz}^{yield} is obtained for the *fully-flexible* system for all cases considered.

The behaviour of P_{xz} as a function of α for each of the three models is shown in Fig. 10. Each point represents a single CBMC simulation at a given registry and constant applied load. For the *fully-flexible* system (Fig. 10(b)), two curves corresponding to $k_\theta = 200$ and $k_\theta = 400$ are shown. The results for untilted brushes (with their director perpendicular to the surface) are shown as solid lines, while the results for the tilted brushes (with their director at an angle of 30° to the normal are shown as dashed lines). The yield point corresponds to the maximum in the domain of $\alpha \in [0.0, 0.5]$.

In the *rigid* and *semi-rigid* models for both tilted and non-tilted systems (Fig. 10(a)), the P_{xz} curves exhibit an approximately parabolic shape with a well defined maximum with $\alpha_{\text{yield}} \approx 0.3$. In the *fully-flexible* model, a static friction point can also be identified, however, as expected, the peak is not so well pronounced as for the more rigid systems. Fur-

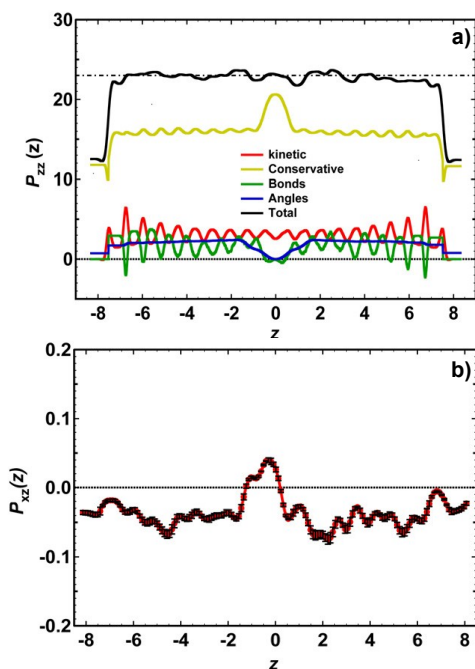


Fig. 9 Pressure tensor profiles: a) different components of the normal pressure tensor, $P_{zz}(z)$, at an imposed load of 23 and b) frictional pressure, $P_{xz}(z)$, corresponding to $\alpha = 0.3$ at an imposed load of $P_{zz}(z) = 27$.

therefore, α_{yield} is lower for the *fully-flexible* model with $\alpha_{\text{yield}} \approx 0.2$. Although it is more difficult to make an accurate estimate of α_{yield} for the *fully-flexible* mode, a reasonably accurate estimate of P_{xz}^{yield} can still be made from the slowly varying $P_{xz}(\alpha)$.

P_{xz}^{yield} for *fully-flexible* < *semi-rigid* < *rigid* and the same order is observed for α_{yield} . The decreased ordering of the polymer brushes at the interface reduces the translational ordering in the monolayers of solvent between the brushes and it takes less force to initiate sliding and sliding can occur at a lower value of the incommensurability. As expected, the higher the value of k_{θ} , the increase in the rigidity of the brushes and the higher the yield stress. $k_{\theta} = 200$ represents a lower limit for this approach. For softer bond-angle potentials the disorder of the polymer chains means that there is no memory of the grafting structure at the interface between the brushes. $k_{\theta} = 400$ represents a higher limit, since the configurational bias method becomes computationally inefficient for higher values of k_{θ} .

The yield stress for the tilted systems is always higher than that of the the untilted system for the models we have considered. In the *rigid* model the rotation of the chains from the surface normal creates a component of the force in

the x-direction, even when the chains are perfectly aligned ($\alpha = 0$ in this case corresponds to geometry in which the tail groups in the upper and lower polymer layers have the same x-coordinate). The mismatch of the alignment increases this force. Recent studies²³ of two crystalline surfaces lubricated by a monolayer of liquid crystal (LC) material show that the friction force is strongly dependent to the orientational ordering of lubricating phase. The mesogens exhibit a significant orientational order in the stick state, and become ordered as the system slips, the extent of disordering being related to the structure of the confining state.

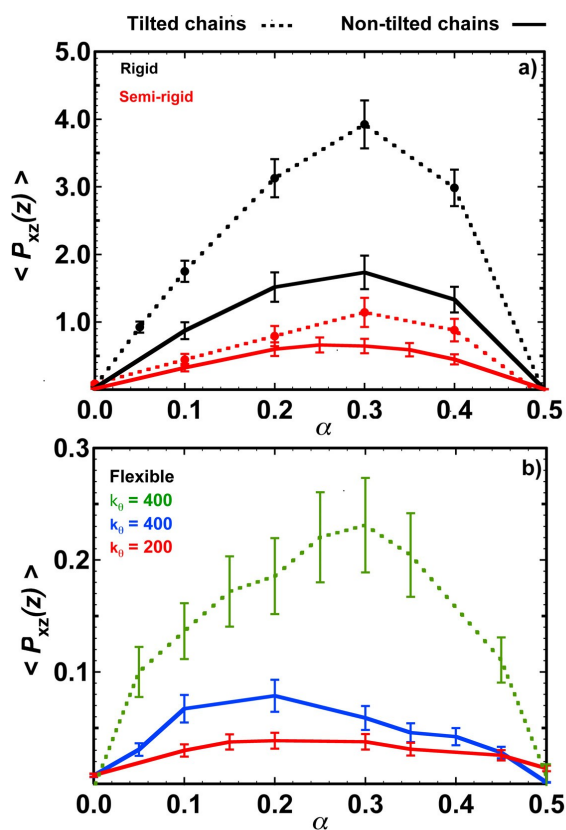


Fig. 10 The frictional force as a continuous function of the registry of the rigid walls for the a) *rigid*, *semi-rigid* and b) *fully-flexible* models in the tilted and untilted structures.

The static friction point at different values of fixed applied load P_{zz} , can be fitted using Amontons' law for adhering surfaces³²:

$$P_{xz}^{\text{yield}} = \mu P_{zz} + P_0 \quad (16)$$

where μ is the static friction coefficient (μ_s) in the case of CBMC simulations, and the kinetic friction coefficient (μ_k) when the DPD simulations are employed. The constant P_0 ap-

pearing in eqn (16) signifies that a finite frictional force arises even in the absence of applied load. This is due to an additional internal load that results from attractive forces between the brushes and between the brushes and the surface. The behaviour of P_{xz}^{yield} as a function of P_{zz} for the three different models in study by CBMC in the non-tilted regime, is plotted in Fig. 11. The DPD simulation results are also plotted, and each point on this curve represents an independent simulation performed at fixed applied load and constant shear rate of $\dot{\gamma}_a = 5 \times 10^{-4}$ in reduced units (note $v_x = L_z \dot{\gamma}_a / 2$).

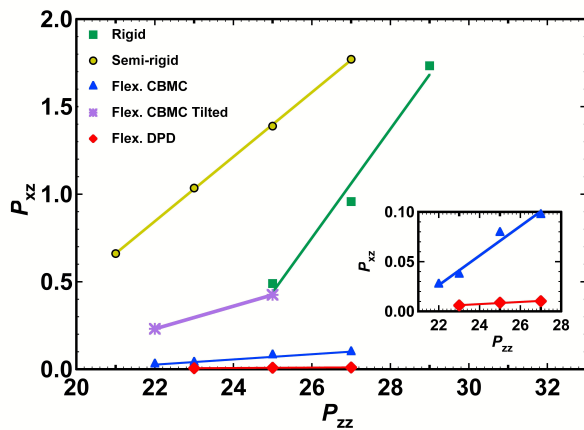


Fig. 11 The static frictional forces P_{xz} as a function of the normal forces P_{zz} , for the *rigid*, *semi-rigid* and *fully-flexible* models in the non-tilted brushes regime. The results of DPD simulations at different values of load and constant shear velocity are also shown. Linear regressions give the coefficients presented in Table 1.

The slope of the curves from the MC simulations are our estimate of the static friction coefficient, and in the case of the DPD simulations of the *fully-flexible* system, it represents the kinetic friction coefficient at that particular sliding velocity. The average components of the pressure tensors, friction coefficients and respective standard deviations, ϵ , are presented in Table 1, as a function of the load. As expected, μ_s decreases significantly when going from the *rigid* to the *fully-flexible* system. This is related to the degree of order in the thin solvent film between the brushes. The more structured (rigid) the brushes the more ordered is the fluid between the surfaces and the higher is the resistance to shear. As observed for most lubricating systems μ_k is smaller than μ_s , reflecting the larger lateral force necessary to initiate the sliding. These results are presented in the form of a Stribeck plot in Fig. 12. Here, the friction coefficient is calculated through eqn (2) since we want to work at a particular normal pressure. We have assumed that the shear viscosity of the entrapped fluid or solvent is constant in constructing the plot. The static friction coefficient was obtained using CBMC at $P_{zz} = 23$. The other points are the result

Table 1 Average components of pressure tensor P_{zz} and P_{xz} , P_{xz}^{yield} , average friction coefficient (μ) and internal pressure (P_0) calculated using eqn (16), for all the systems in the study.

P_{zz}	α_{yield}	$-P_{xz}^{\text{yield}}$	$P_0 \pm \epsilon$	$\mu_s \pm \epsilon$
rigid				
25	0.20	0.489		
27	0.25	0.958	-7.336 ± 1.202	0.311 ± 0.044
29	0.30	1.733		
semi-rigid				
21	0.25	0.661		
23	0.30	1.035	-3.205 ± 0.042	0.184 ± 0.002
25	0.25	1.389		
27	0.30	1.770		
fully-flexible - CBMC				
22	0.30	0.027		
23	0.10	0.037	-0.300 ± 0.044	0.015 ± 0.002
25	0.20	0.079		
27	0.35	0.097		
fully-flexible tilted - CBMC				
22	0.30	0.231	-1.192 ± 0.001	0.065 ± 0.003
25	0.30	0.425		
fully-flexible - DPD				
P_{zz}	$\dot{\gamma}_a \cdot 10^4$	$P_{xz} \cdot 10^3$	$(P_0 \pm \epsilon) \cdot 10^2$	$(\mu_k \pm \epsilon) \cdot 10^3$
23		12.9		
25	10	17.5	-3.6 ± 0.24	2.1 ± 0.09
27		21.4		
23		5.97		
25	5	8.76	-1.9 ± 0.46	1.1 ± 0.18
27		10.3		
23		3.98		
25	2.5	4.88	-0.6 ± 0.02	0.4 ± 0.01
27		5.71		

of the DPD simulations at different values of load and shear velocities (Table 1). The fundamental shape of the Stribeck curve (as sketched in Fig. 1) is visible in Fig. 12, if we ascribe the static friction coefficient as the limit of the boundary layer friction and take the results from the DPD simulations for the hydrodynamic lubrication regime. We note that the use of the friction coefficient from the slopes would result in a similar curve with lower values of μ_k . The values μ_k obtained at lower sliding velocities are comparable with the experimental estimates for this system of $(1.5 \pm 1) \times 10^{-3}$, as suggested by Chen *et al.*⁷. The ratio of μ_k/μ_s for the *fully-flexible* model changes from 0.11 to 0.5 over the range of shears rates studied. Experimentally this ratio is close to 0.5 for solid surfaces

lubricated by oils³ and given the simplicity of our model, the model results are in reasonable agreement with experiment. The nature of the two simulation techniques means that we are not able to reproduce any point in the mixed lubrication regime with these methods so it is not possible to claim that we have reproduced the Stribeck curve, although we have captured its limiting features.

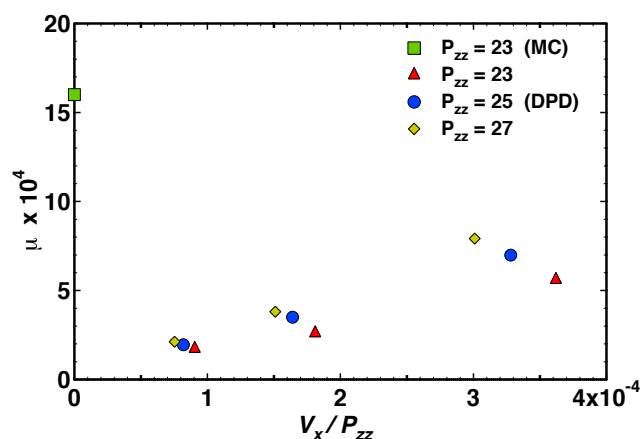


Fig. 12 The combination of the CBMC and DPD results for *fully-flexible* model. The DPD results are calculated for normal pressure of 23, 25 and 27. The friction at a particular normal pressure are calculated from eqn (2)

5 Conclusions

A quasistatic approach, originally developed for molecularly thin Lennard-Jones fluids confined between parallel walls, has been successfully applied to a system of end-grafted polymer brushes immersed in solvent to calculate the static friction coefficient of the system. Simple models have been developed which are compatible with a polyzwitterionic brushes of poly[2-(methacryloyloxy) ethyl phosphorylcholine] (pMCP), in aqueous media, at physiological pressures (up to 7.5 MPa), where the friction coefficient has been measured using the surface forces apparatus. That is to say the models reproduce the correct brush width to polymer separation of the real system, along with a reasonable value of the normal pressure and they predict values of both the static and kinetic friction of the same magnitude as those observed in the experiment. Our purpose is not to try to model the atomistic detail of the layer but to create three general models that can be used to study the effect on the static friction as the layers becomes more structurally disordered.

In previous studies, we have shown that non-equilibrium DPD simulations can only predict the kinetic friction coefficients at relatively high sliding velocities and low normal

loads and this method does not allow us to reach the boundary layer regime. In this work, we present a configurational bias Monte Carlo method for measuring the static friction by looking at the tangential component of the pressure induced by a mismatch in the registry of the two grafting surfaces.

We have successfully calculated the static friction coefficient for three model systems of grafted polymers which exhibit increasing intramolecular flexibility. These are: the totally rigid brushes (combs moving through a disordered solvent); a model involving additional bond-stretching which creates disorder in the direction normal to the polymer-polymer interface; and a model involving additional bond angle and torsional distortions, which creates additional lateral disorder in the plane of the interface. The third of these is the most realistic representation of the experimental system under consideration. Our results show that slip occurs at much lower values of shear force the more flexible the polymer layer. A moderate increase in the flexibility of the chains reduces the friction coefficient by a factor of ca. 20. Most of this change is associated with bond-angle and torsional distortion in the *fully-flexible* model. In addition, we have studied the initial orientation of the brushes at zero shear on the static friction by simulating models where the director of the polymer brushes is tilted by an angle of 30° with respect to the walls. The tilting increases the value of P_{xy}^{yield} and produces an increased friction coefficient where the top, tilted layer is displaced in the direction away from the tilt.

The behaviour of P_{xz} in function of the registry of the walls was calculated for all models, at different values of applied load and Amonton's law, which is obeyed by these systems, was used to calculate the static friction coefficient.

Non-equilibrium dynamics techniques using the same model were performed using DPD and the limiting extremes of the Stribeck curve associated with the boundary lubrication regime and the hydrodynamic lubrication regime were observed. As expected, μ_k is significantly lower than μ_s for the same system. The dynamical friction coefficients in the model are in good agreement with those observed in the experiment and the ratio of μ_k/μ_s of between 0.11 and 0.5 is close to the values of 0.5 normally seen for these systems. It is interesting that this behaviour can be observed in simple models of perfectly flat surfaces with grafted polymers without the introduction of surface asperities. In future work, we plan to introduce surface asperities at different length scales to study the effect of surface inhomogeneity on static and kinetic friction and to study the effect of increasing the normal load at low sliding velocity to try to observe the mixed lubrication regime by non-equilibrium simulation.

6 Appendix

The wall is modelled as a continuum solid composed of DPD atoms at a uniform density ρ_w . The interaction potential between a particle i in the bulk (solvent or polymer) and a volume element, jw , is $v_{i,jw}^C(r)$; (the conservative DPD potential is defined in eqn. (5)). As shown in Fig. (13), the plane containing the first layer of wall particles is at $Z = 0$ and i is at a distance z from this plane and jw and i are separated by r .

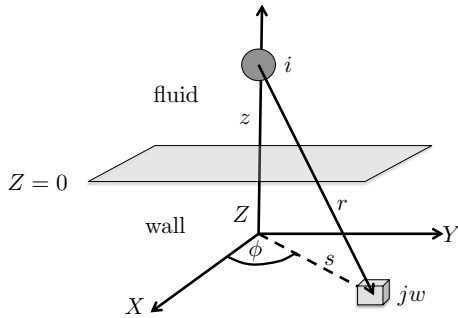


Fig. 13 Coordinate system for the wall-fluid particle potential,

The potential energy between particle i and the wall is

$$V_{i,w}(z) = \int_{-\infty}^{+\infty} dX \int_{-\infty}^{+\infty} dY \int_0^{+\infty} dZ v_{i,jw}^C(r) \rho_w. \quad (17)$$

Changing from cartesian to the cylindrical coordinates, and noting that the conservative part of the DPD potential for $r_c = 1$ is

$$v_{i,jw}^C(s, z+Z) = \frac{a_{iw}}{2} \left(\sqrt{(z+Z)^2 + s^2} - 1 \right)^2 \quad r < 1$$

$$= 0 \quad z+Z > 1$$

$$= 0 \quad s^2 \geq 1 - (z+Z)^2 \quad (18)$$

we can integrate over ϕ to obtain

$$V_{i,w}(z) = \pi a_{iw} \rho_w \int_0^{1-z} dZ \int_0^{\sqrt{1-(z+Z)^2}} s ds$$

$$\times \left(\sqrt{(z+Z)^2 + s^2} - r_c \right)^2 \quad (19)$$

and finally

$$V_{i,w}(z) = \pi a_{iw} \rho_w \left[\frac{1}{30} - \frac{z}{12} + \frac{z^3}{6} - \frac{z^4}{6} + \frac{z^5}{20} \right] \quad (20)$$

where a_{iw} is the repulsive parameter between a wall and fluid particle. The force in eqn (6) is the negative of the derivative of eqn (20) with respect to z .

References

- 1 D. Dowson, *History of Tribology*, Wiley, New York, 2nd edn., 1997.
- 2 X. Lu, M. M. Khonsari and E. R. M. Gelinck, *J. Tribology - Trans. ASME*, 2006, **128**, 789–794.
- 3 B. Persson, *Sliding Friction: Physical Principles and Applications*, Springer, Berlin, 2nd edn., 2000.
- 4 F. Goujon, A. Ghoufi, P. Malfreyt and D. J. Tildesley, *Soft Matter*, 2012, **8**, 4635–4644.
- 5 F. Goujon, A. Ghoufi, P. Malfreyt and D. J. Tildesley, *Soft Matter*, 2013, **9**, 2966–2972.
- 6 R. Groot and P. Warren, *J. Chem. Phys.*, 1997, **107**, 4423–4435.
- 7 M. Chen, W. H. Briscoe, S. P. Armes and J. Klein, *Science*, 2009, **323**, 1698–1701.
- 8 M. Schoen, S. Hess and D. J. Diesteler, *Phys. Rev. E*, 1995, **52**, 2587–2602.
- 9 P. Bordarier, B. Rousseau and A. H. Fuchs, *J. Chem. Phys.*, 1997, **106**, 7295–7303.
- 10 N. Marom, J. Bernstein, J. Garel, A. Tkatchenko, E. Joselevich, L. Kronik and O. Hod, *Phys. Rev. Lett.*, 2010, **105**, 046801.
- 11 O. Hod, *Phys. Rev. B*, 2012, **86**, 075444.
- 12 O. Hod, *ChemPhysChem*, 2013, **14**, 2376–2391.
- 13 I. Leven, D. Krepel, O. Shemesh and O. Hod, *J. Phys. Chem. Lett.*, 2013, **4**, 115–120.
- 14 K. Kremer and G. S. Grest, *J. Chem. Phys.*, 1990, **92**, 5057–5086.
- 15 P. A. Thompson and M. O. Robbins, *Science*, 1990, **250**, 792–794.
- 16 G. He, M. H. Muser and M. O. Robbins, *Science*, 1999, **284**, 1650–1652.
- 17 G. He and M. O. Robbins, *Phys. Rev. B*, 2001, **64**, 035413.
- 18 B. Persson, O. Albohr, F. Mancosu, V. Peveri, V. Samoilov and I. Sivebaek, *WEAR*, 2013, **254**, 835–851.
- 19 J. I. Siepmann and D. Frenkel, *Molec. Phys.*, 1992, **75**, 59–70.
- 20 B. Smit, *Molec. Phys.*, 1995, **85**, 153–172.
- 21 M. Griebel, S. Knapek and G. Zumbusch, *Numerical Simulation in Molecular Dynamics: Numerics, Algorithms, Parallelization, Applications (Texts in Computational Science and Engineering)*, Springer, 2007.
- 22 D. Irfachsyad, D. Tildesley and P. Malfreyt, *Phys. Chem. Chem. Phys.*, 2002, **4**, 3008–3015.
- 23 W. Chen, S. Kulju, A. S. Foster, M. J. Alava and L. Laurson, *Phys. Rev. E*, 2014, **90**, 012404.
- 24 F. Goujon, P. Malfreyt and D. J. Tildesley, *ChemPhysChem*, 2004, **5**, 457–464.
- 25 B. Widom, *J. Stat. Phys.*, 1978, **19**, 563–574.
- 26 J. Irving and J. Kirkwood, *J. Chem. Phys.*, 1950, **18**, 817–829.
- 27 J. Walton, D. Tildesley, J. Rowlinson and J. Henderson, *Molec. Phys.*, 1983, **48**, 1357–1368.
- 28 H. Heinz, W. Paul and K. Binder, *Phys. Rev. E*, 2005, **72**, 066704.
- 29 M. Schoen, D. J. Diesteler and J. H. Cushman, *J. Chem. Phys.*, 1994, **100**, 7707–7717.
- 30 P. Espanol and P. Warren, *Europhys. Lett.*, 1995, **30**, 191–196.
- 31 M. L. Gee, P. M. McGuiggan, J. N. Israelachvili and A. M. Homola, *J. Chem. Phys.*, 1990, **93**, 1895–1906.
- 32 H. Yoshizawa, Y. I. Chen and J. Israelachvili, *J. Phys. Chem.*, 1993, **97**, 4128–4140.

A configurational bias Monte Carlo method has been developed to calculate the static friction between two grafted polymer brushes.

